Delft University of Technology

Experimental research on the determination of the coefficient of sliding wear under iron ore handling conditions

Chen, G.; Liu, Yueting; Lodewijks, Gabri; Schott, Dingena

Important note
To cite this publication, please use the final published version (if applicable).
Please check the document version above.

Tribology in Industry

Experimental Research on the Determination of the Coefficient of Sliding Wear under Iron Ore Handling Conditions

G. Chen[a], Y. Liu[b], G. Lodewijks[c], D.L. Schott[a]

[a]*Department of Maritime and Transport Technology, Delft University of Technology, Mekelweg 2, Delft, Netherlands,*
[b]*Department of Precision and Microsystems Engineering, Delft University of Technology, Mekelweg 2, Delft, Netherlands,*
[c]*School of Aviation, the University of New South Wales, Sydney, NSW 2052, Australia.*

Corresponding author:

G. Chen
Department of Maritime and
Transport Technology,
Delft University of Technology,
Mekelweg 2, Delft,
Netherlands.
E-mail: guangming2012@hotmail.com

A B S T R A C T

The handling of iron ore bulk solids maintains an increasing trend due to economic development. Because iron ore particles have hard composites and irregular shapes, the bulk solids handling equipment surface can suffer from severe sliding wear. Prediction of equipment surface wear volume is beneficial to the efficient maintenance of worn areas. Archard's equation provides a theoretical solution to predict wear volume. To use Archard's equation, the coefficient of sliding wear must be determined. To our best knowledge, the coefficient of sliding wear for iron ore handling conditions has not yet been determined. In this research, using a pin-on-disk tribometer, the coefficients of sliding wear for both Sishen particles and mild steel are determined with regard to iron ore handling conditions. Both naturally irregular and spherical shapes of particles are used to estimate average values of wear rate. Moreover, the hardness and inner structures of Sishen particles are examined, which adds the evidence of the interpretation of wear results. It is concluded that the coefficients of sliding wear can vary largely for both Sishen particle and mild steel. The wear rate decreases from transient- to steady-state. The average coefficient of sliding wear is capable of predicting wear with respect to long distances at the steady-state. Two types of sliding friction are distinguished. In addition, it is found that the temperature rise of the friction pairs has negligible influence on wear rate.

1. INTRODUCTION

Iron ore is used as a raw material for steel-making companies. Driven by economic developments, the demand of steel products increases, which gives rise to the increasing supply of iron ore, resulting in a large-scale iron ore handling industry. Due to the hard composites and irregular shapes of iron ore particles [1], the surfaces of bulk solids handling equipment can suffer from severe sliding wear by particles [2]. Wear reduces surface thickness

and thus accelerates the damage of bulk solids handling equipment surface. When the worn areas of equipment surface can be accurately predicted, the efficient maintenance strategies can be applied, and thus that maintenance cost and downtime can be reduced.

In bulk solids handling, Sishen iron ore [1] is one of the most demanded ore types and many equipment surfaces that handle iron ore are made of mild steel. Therefore, in this research Sishen iron ore particles and mild steel are used. For the sliding wear of mild steel, Archard's equation [3] can be used to predict wear volume W_V, which is given as,

$$W_V = (K/H)F_n l = \alpha_s F_n l \qquad (1)$$

where K is a factor which depends on the combination of wear bodies; H is the hardness of the worn surface; F_n is normal force and l is sliding distance. The parameter α_s denotes as coefficient of sliding wear ($\alpha_s = K/H$). To apply equation (1) to predict sliding wear volume, the coefficient of sliding wear α_s must be investigated.

In the research related to the coefficient of sliding wear α_s, Challen, et al. [4] derived a formula to express K for a hard asperity sliding against metallic materials based on a low cycle fatigue mechanism. It was obtained that K varies largely from smooth (and/or lubricated) surface to rough (and/or unlubricated) surface. Using the low cycle fatigue mechanism and the slip-line fields, Lacey and Torrance [5] express K differently with respect to the low and the high slopes. This work confirmed that K increases dramatically with increasing contact friction. In addition, Yang [6,7] developed an equation of K that can predict sliding wear for both transient-state and steady-state. Ramesh, et al. [8] implemented the K developed by Yang [6,7] and found that the predicted wear volumes are slightly lower than the experiments of Al6061–TiO$_2$ composites [8].

Recently, Amiri, et al. [9] theoretically predict that the average K is in the order of 10^{-4} for the wear of steel with respect to the counterparts bronze and brass. Yau, et al. [10] obtained that the coefficient K is in the order of 10^{-7} for gold wire wear by a silicon wafer using a very low normal force (5 μN).

The above literature review highlights the research for the factor of K. For the wear counterpart of Sishen iron ore particles, Taylort, et al. [1] reported the average chemical composition of the Sishen particles. Siemes [11] investigated the microstructure and texture. However, the hardness of Sishen iron ore particles has not yet reported. To conclude, the coefficient of sliding wear α_s (K/H) under iron ore handling conditions has not been determined.

The goal of this paper is to determine the coefficient of sliding wear under bulk solids handling conditions. To carry out sliding wear test of a friction pair, a pin-on-disk configuration [12-15] is widely used. To use a pin-on-disk apparatus to perform particle sliding wear, a particle can be mounted on the pin end. To account for the wear characteristics by different particle asperities, the particles with naturally irregular shapes and spherical shapes must be used [16]. Accordingly, the spherical particles are fabricated. The hardness and inner structures of Sishen particles are examined such that wear results can be more confidently interpreted [17]. To distinguish wear from transient to steady states, different sliding distances [7] must be implemented. Moreover, the effects of sliding speed [18,19] are studied. In addition, the sliding friction and temperature rise [20,21] are analyzed.

2. MATERIALS AND METHOD

This section firstly presents the material properties of Sishen iron ore and mild steel. After that, the experimental setup is presented. Then the experimental plan and the samples for the sliding wear tests are shown. Finally, the procedure for determining the coefficient of sliding wear is presented.

2.1 Material Properties

Figure 1 shows a sample of Sishen iron ore bulk solid. It can be seen that Sishen particles are of variously irregular shapes. Figure 1a shows its particle size distribution by mass [22], which was obtained by sieving samples. The used sieve sizes were 8, 4, 2.4, 1.7, 1 and 0.5 mm [22]. The maximum particle size $d_{max} \approx 18$ mm the median diameter $d_{50} = 3$ mm. Using a gas-expansion pycnometer, the average density of Sishen

particles ρ_p is measured to be 4865 ±72kg/m³ (using 95 % confidence interval), which accounts for relatively big and relatively small particles. The density of the used mild steel is measured at 7932 kg/m³.

a)   b)
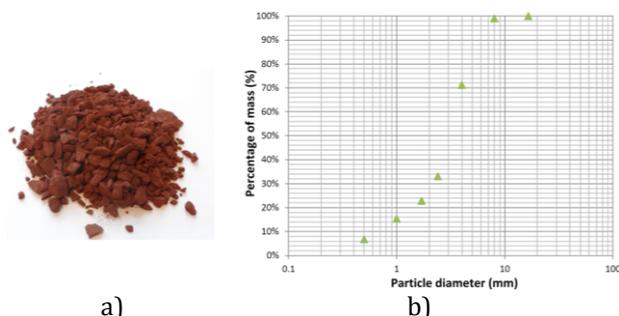
Fig. 1. A bulk solid sample (a) Sishen iron ore and (b) particle size distribution [22].

To measure hardness of the Sishen particles and the mild steel, the surfaces of selected particles and mild steel are prepared by sanding and polishing. The obtained surface roughness is less than 1 μm, and fits for micro-hardness test.

Figures 2a and 2b shows a visual of the appearance of inner structure of a Sishen particle before and after a hardness test under a microscope, in which the white color represents the solid material and the black represents the porosity between materials. It can be seen that the inner structure of Sishen particle is porous and inhomogeneous. Furthermore, cracks are observed from the inner surface. The applied normal force for indentation test is estimated based on the pressure on equipment surface under bulk solids handling conditions [2]. Referring to the scales of our Vickers hardness test apparatus, a normal force 9.8 N is selected. Because it is a relatively low force, the hardness tests had to be performed on particle surface surfaces of relatively homogenous structures and without cracks. Otherwise, imprecise measurements of indention areas are caused, which results in unreliable hardness data.

Figure 3 shows the Vickers hardness number obtained from 8 relative big and 12 relative small Sishen particles. Each surface was tested eight times at the center and other eight times at the edge. Thus totally 320 tests were done on the 20 particles. The same color data are Vickers numbers from one particle surface. Therefore the hardness measurements are varied by tested areas and particles.
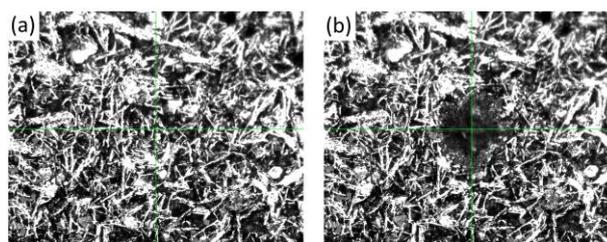
Fig. 2. Appearance of the inner structure of a Sishen particle (400×) (a) before hardness test (b) after hardness test.
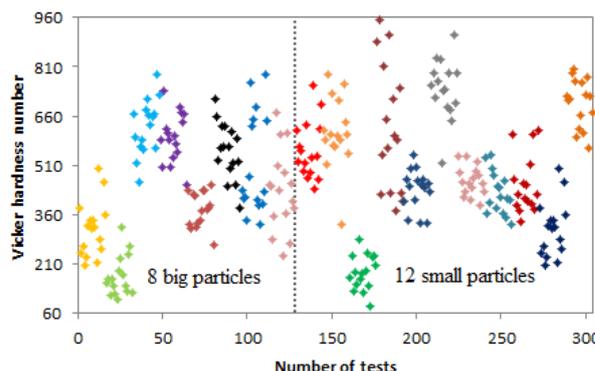
Fig. 3. Sishen particle hardness from 320 tests using 8 big and 12 small sizes.

Using 95 % confidence interval, the Vickers hardness number of Sishen particles is 476 ±19. The frequency distribution of the Vickers hardness of Sishen iron ore is shown in Fig. 4. The Vickers hardness number of mild steel is measured as 143 ±4 (95 % confidence interval). It can be estimated the hardness ratio between particle and disk $0.15 < H_p/H_d < 2.4$, which indicates that wear rate of particles can deviate largely with respect to such large range of hardness ratio [17]. Besides, it is calculated that a possibility of 94 % for $1.2 < H_p/H_d < 6.7$, which corresponds to heavy wear [3,17].
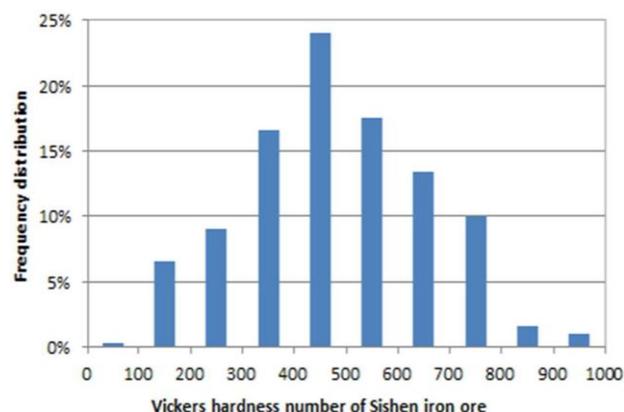
Fig. 4. Frequency distribution of Vickers hardness number of Sishen iron ore.

2.2 Experimental Setup

Figure 5 shows the apparatus of a laboratory pin-on-disk tribometer. An infrared camera is implemented to measure surface temperature during the dry sliding wear process.
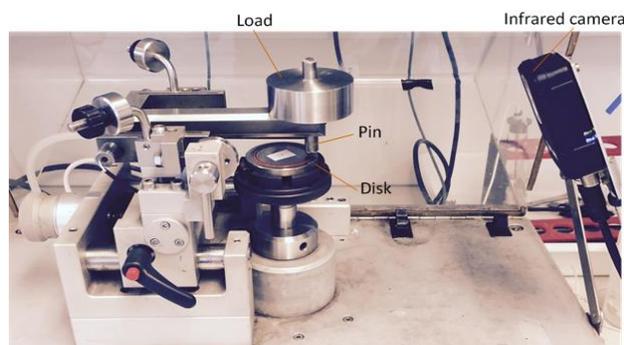
Fig. 5. A pin-on-disk tribometer and an infrared camera.

The driving power used for rotational disk is provided by an electric motor. As the disk rotates, the sliding motion generates between the pin and the disk surface. To perform the sliding wear by a particle, the particle is attached on the pin end. The standard test method [12] is followed to conduct a pin-on-disk wear test. The infrared camera is used to measure surface temperature at the proximity of contact between particle tip and mild steel disk. The accuracy of the measured temperature is ±0.1 ºC.

2.3 Experimental plan

As mentioned earlier, the investigated parameters are particle shape, sliding distance, sliding speed, and normal force. Table 1 presents the experimental plan which is determined based on the references of bulk solids handling conditions. It is noted that the range of sliding speed is smaller than practice. This is because for higher rotating speeds, severe vibration between the pin and disk is triggered, which can lead to incorrect results of the sliding wear.

In series I of Table 1, the tests No. 1-8 and No. 25-26 respectively correspond to eight natural particle tips and two spherical tips. In series II, each particle in tests No. 9-16 is used once and corresponds to one distance. By contrast, each particle in tests No. 27-28 is used for multiple times and corresponds to a series of distances. The tests No. 17-20 are used to examine the effects of different sliding speeds on wear. To minimize the contact difference between pin and

disk, similar shapes of particle tips are selected. The tests No. 21-24 are used to obtain wear volumes subjected to different indentation forces, in which similar shapes of particles are also used.

Table 1. Experimental plan of pin-on-disk wear test.

Series	Test No.	Wear parameters	Variances	Base values
I	1-8; 25-26	particle shapes [-]	non-spherical; spherical	-
II	9-16; 27-28	sliding distance l [m]	9-225	180
III	17-20	sliding speed v [m/s]	0.05-0.25	0.15
IV	21-24	normal force F_n [N]	1-10	5

2.4 Test samples

Figure 6 shows the 28 pins corresponding to the experimental plan. The used cylindrical parts for making the 28 pins are identical. For each test, a pin is fixed at a distance of 22 mm with respect to the axis of the rotational disk. The two spherical particles (No. 25-26) were fabricated by laser carving where water was used as cooling agent.

Fig. 6. Particle pins used for pin-on-disk wear test.
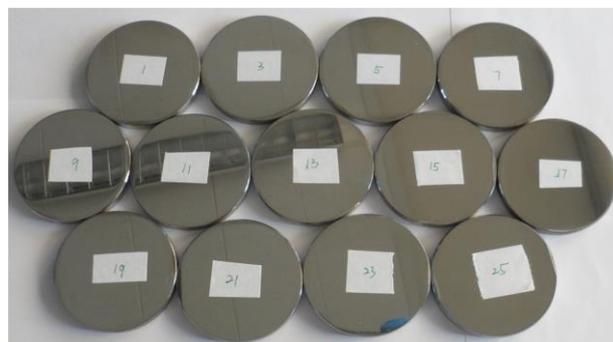
Fig. 7. Samples of mild steel disk for pin-on-disk wear test.

Figure 7 shows the samples of prepared mild steel disks. Each sample was prepared as that used for hardness test. The radius and thickness of all disks are 26.5 mm and 6 mm respectively. During the tests, each pin was used with a specific side of a mild steel disk.

2.5 Analysis Procedure

Due to the fact that contact area varies during a sliding test, the wear morphologies on the mild steel disk surface is inhomogeneous, which makes it difficult to calculate wear volumes when using wear profiles of the wear path. Alternatively, a laboratory electron balance (with the accuracy of ±0.5 mg) can be used to measure the mass of mild steel and particle before and after each test. Thus the volume of wear W_V can be calculated by using equation (2),

$$W_V = \frac{m_0 - m_1}{\rho} \qquad (2)$$

where m_0 and m_1 are respectively the measured mass of worn material before and after test, and ρ is the density of worn material. The coefficient of sliding wear α_s for both Sishen particle and mild steel will be estimated using equation (3) which is derived from equation (1). The error range for α_s can be obtained using error propagation rules, which reprocesses the standard deviations introduced by the measured mass and density.

$$\alpha_s = \frac{W_V}{F_n\, l} \qquad (3)$$

3. RESULTS AND DISCUSSIONS

Previous section outlines the materials and the experimental method for particle sliding wear test. In this section, the results of the pin-on-disk wear tests are discussed. It is referred to Table 1 for the experimental plan. Using the test results and Archard's equation (1), the coefficients of sliding wear for both particle and mild steel surface are determined. Furthermore, the sliding friction and temperature rise are characterized.

3.1 Wear Subjected to Different Particle Tips: Series I

Figure 8 shows the particle morphologies of before tests (No. 1-8) and after tests (No. 1'-8'). The blue color area on particle tips was made to

assist identification of worn surface under microscope. It can be seen that some particles have notable differences after tests (i.e., No. 2', 6', and 7'), which means that these particles have substantial wear loss. By comparison, others have insignificant changes and thus less wear loss.
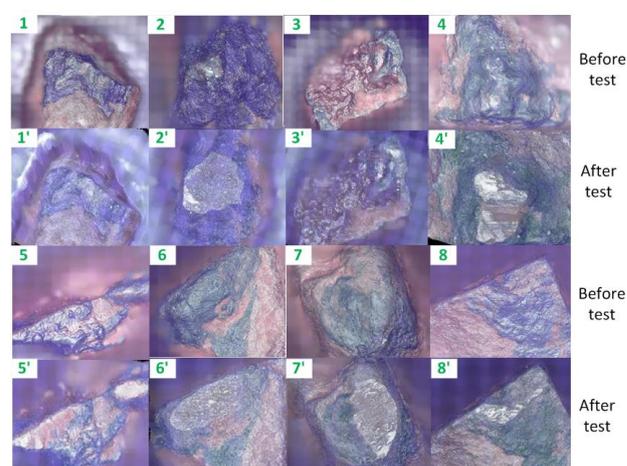
Fig. 8. Morphologies of irregular particle tips before tests (No. 1-8) and after tests (No. 1'-8').

Figure 9 shows the wear morphologies of the two spherical particles before tests (No. 25-26) and after tests (No. 25'-26'). The surface of No. 25' appears red and compared to other particles, a substantial amount of material was worn off from this particle. The reason for the high wear is believed that No. 25 particle has porous structure and oxidation material due to water being used during fabricating process. To obtain a reliable value for evaluating the dry sliding wear in iron ore handling, the results of the test No. 25 are discarded.
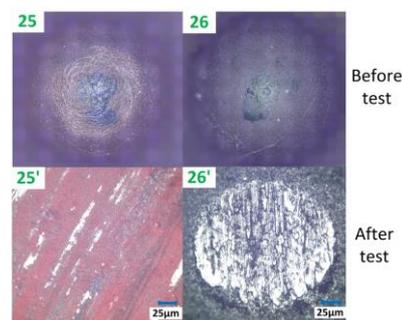
Fig. 9. Morphologies of spherical particle tips before tests (No. 25-26) and after tests (No. 25'-26').

Figure 10 shows an example of wear morphology of a mild steel disk surface. During a sliding wear process, grooves are formed as a result of the removal and the transfer of mild steel surface material. Figure 10(a) shows an

area of the wear path and a line to measure the wear profile of a cross-sectional area. Figure 10(b) illustrates the three-dimensional (3D) wear morphology. Figure 10(c) presents the obtained profile from the measured cross-section. Because of the inhomogeneous wear morphology, the wear profile consequently changes with respect to the measurements at different locations.
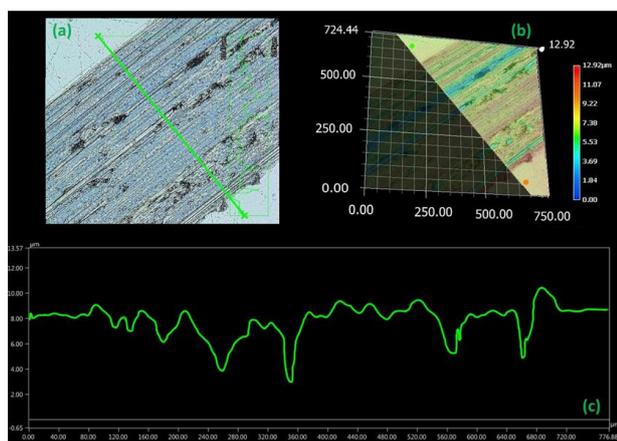
Fig. 10. Wear morphology of a mild steel disk surface (a) an area of wear path; (b) 3D visualization; (c) profile of the measured cross-section area.
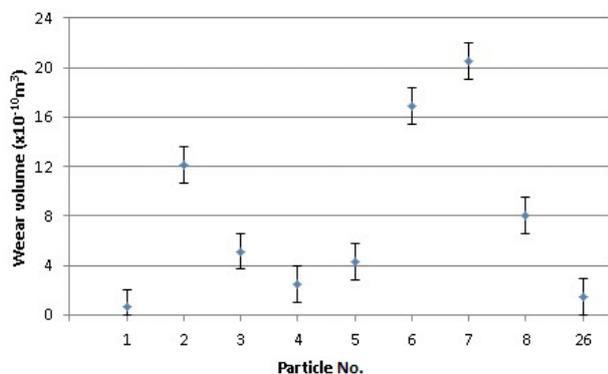
Fig. 11. Wear of particles of No. 1-8 and 26.
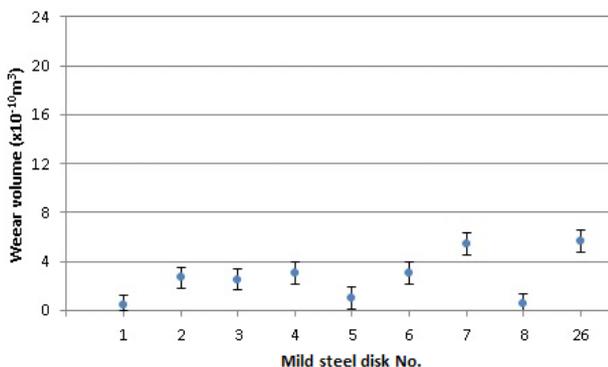
Fig. 12. Wear volume of mild steel of No. 1-8 and 26.

Figures 11 and 12 shows the wear volumes of particles and mild steel disks for tests No. 1-8

and 26. It can be seen that the wear volumes deviate from each test for both particle and mild steel disk. According to Archard's equation (1), the deviation of wear volumes can be partially attributed to the different shapes of particle tips which causes different contact areas and thus affects the coefficient K [20,24]. However, the main reason is likely the difference in particle hardness (Fig. 3) according to Archard's equation (1). By comparison, the deviation of the volume loss of particles is higher than that of mild steel disk, which is due to the high variation of H_d/H_p (which was illustrated in section 2.1) that dominates the wear rate [17].

Figures 11 and 12 also demonstrate that the average wear volume for particles is higher than that of steel disks. The reason is ascribed to the porous structure and the cracks of the Sishen particles, which triggers damages to the inner structure during test, and thus accelerates the wear of particles significantly. Therefore, the particles suffer more wear than the steel disks.

With the obtained wear volumes (Figs. 11 and 12) and the applied base values (Table 1), it is estimated that the average volume of particles is $(7.95 \pm 0.49) \times 10^{-10}$ m³. Using equation (3), the average coefficient of sliding wear for particle $\alpha_{s,p}$ is calculated to be $(8.83 \pm 0.67) \times 10^{-13}$ m²/N. In the same way, the wear volume for the mild steel is obtained at $(5.67 \pm 0.89) \times 10^{-10}$ m³ and the average coefficient of sliding wear $\alpha_{s,d} = (2.99 \pm 0.36) \times 10^{-13}$ m²/N.

3.2 Wear Subjected to Different Sliding Distances: Series II

Figures 13 and 14 shows the wear volumes of particles and mild steel disks of tests No. 9-16. It can be seen that the wear volumes do not always increase when increasing sliding distance. This seems contradicted with the expectation that the wear volume increases with increasing sliding distance [7]. Notably, in the test No. 14 the particle has a remarkably high volume whereas the mild steel disk has a very low volume. The reason for this contradiction is believed to be related to the shapes of particle tips [16]. However, the difference in particle inner structure and hardness can be also possible reasons.
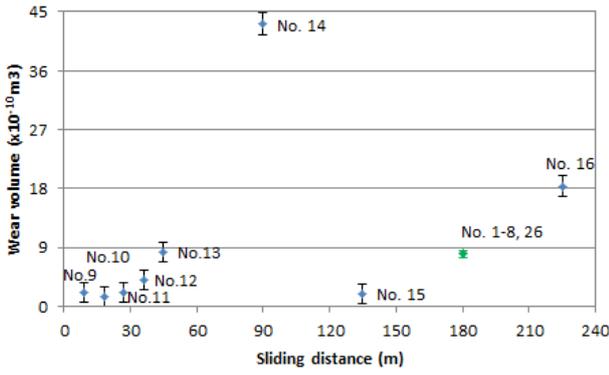
Fig. 13. Wear volume of different particles with respect to sliding distance.
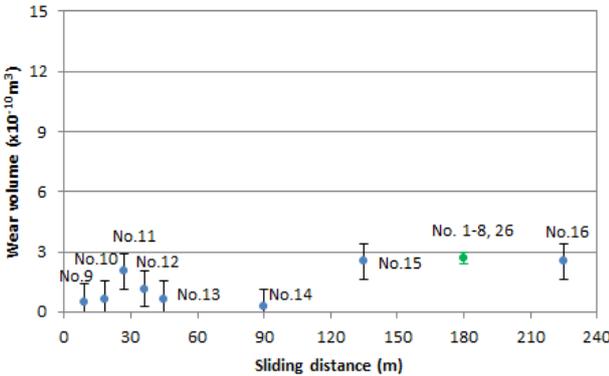
Fig. 14. Wear volume of different mild steel disks with respect to sliding distance.

To verify the influence of inner structure and hardness of No. 14 particle on wear, the micro structure of particle No. 14 was examined after test, as shown in Fig. 15. It can be seen that the inner structure of No. 14 particle is quite porous, which is responsible for the high wear volume of the particle [16,24]. The hardness of this particle is measured in 443 ±45 (based on 16 test points and using 95 % confidence interval). This value is no higher than the average in comparison with the frequency distribution of Sishen particles (Fig. 4), in combination with the porous structure of the particle, it implies that the hardness of No. 14 particle can have a low wear rate of mild steel.
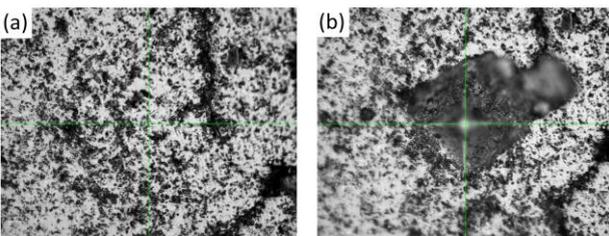
Fig. 15. Hardness test of the worn particle of No. 14 (400×) (a) appearance of inner structure before hardness test (b) after hardness test.

To avoid the influence of the shape, the inner structure, and the hardness of particle on wear, tests No. 27-28 were carried out to examine the correlation between wear volume and siding distance. Figures 16 and 17 show the results of wear volumes for particles and mild steel disks. It can be seen that the wear volumes of both particle and mild steel disk maintain the increasing trend with increasing sliding distance. This result is consistent with Archard's equation (1). The wear volumes for the two particles are comparably equal, whereas notable difference exists between the wear volumes of No. 27 and No. 28 mild steel disks. Referring to Archard's equation (1), the reason for the volume difference of mild steel disks is believed to be the contact difference as a result of different particle shapes that can affect the coefficient K [15,22].
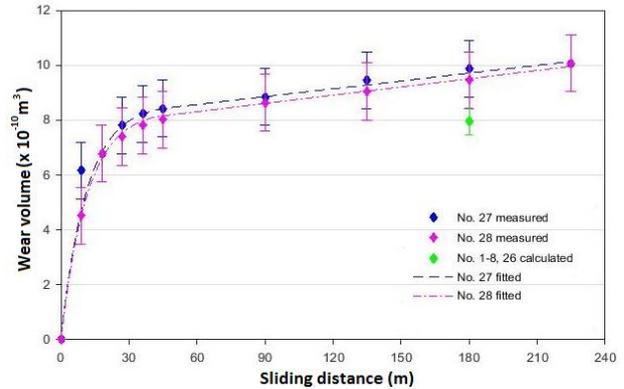
Fig. 16. Wear volumes of No. 27-28 particles as functions of sliding distance.
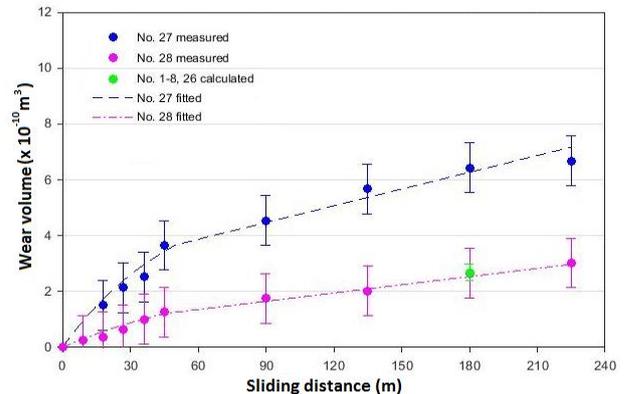
Fig. 17. Wear volumes of No. 27-28 mild steel disks as functions of sliding distance.

In comparison with the average wear volumes obtained for tests No. 1-8 and 26 at the sliding distance 180 m, the wear volumes for both particle and mild steel disks in the tests No. 27-28 are slightly higher. The reason is that in tests No. 27-28 wear debris was cleaned to weigh the

mild steel disk after each test, thus that particle had fresh contact with mild steel disk for next sliding distance. This can initiate a transient-state which corresponds to a higher wear rate than that of the steady-state [6].

For the wear at the transient-state, the wear volume $W_{V,t}$ can be evaluated by [7],

$$W_{V,t} = B(1 - e^{-Cl_t}) \qquad (4)$$

in which B and C are two constants; lt is the distance of the transient-state. The wear volume for the steady-state can be calculated by using Achard's equation (1). Accordingly, the equations for predicting wear volumes of particles $W_{V,s,p}$ and mild steel disks $W_{V,s,d}$ in the tests 27-28 are obtained as shown below.

No. 27 particle,

$$W_{V,s,p} = \begin{cases} 8.58 \times (1 - e^{-0.088l_t}) \times 10^{-10}, & 0 < l_t \leq 50 \\ (0.0095 \times l_s + 8.0) \times 10^{-10}, & 50 < l_s \leq 225 \end{cases} \qquad (5)$$

No. 28 particle,

$$W_{V,s,p} = \begin{cases} 8.35 \times (1 - e^{-0.086l_t}) \times 10^{-10}, & 0 < l_t \leq 45 \\ (0.01 \times l_s + 7.71) \times 10^{-10}, & 45 < l_s \leq 225 \end{cases} \qquad (6)$$

No. 27 disk,

$$W_{V,s,d} = \begin{cases} 5.98 \times (1 - e^{-0.019l_t}) \times 10^{-10}, & 0 < l_t \leq 50 \\ (0.02 \times l_s + 2.67) \times 10^{-10}, & 50 < l_s \leq 225 \end{cases} \qquad (7)$$

No. 28 disk,

$$W_{V,s,d} = \begin{cases} 2.73 \times (1 - e^{-0.013l_t}) \times 10^{-10}, & 0 < l_t \leq 45 \\ (0.098 \times l_s + 0.77) \times 10^{-10}, & 45 < l_s \leq 225 \end{cases} \qquad (8)$$

3.3 Wear Subjected to Different Sliding Speeds: Series III

Figures 18 and 19 shows the wear volumes of particles and mild steel disks for the tests No. 17-20. The wear volumes of particles show a large deviation. Notably, No. 17 particle gives a very high wear volume. However, according to Straffelini, et al. [25], the wear volumes should not vary significantly for the low sliding speeds (0.05-0.10m/s). Here it is likely that the inner structure or particle hardness could affect wear volumes based on the fact that relatively similar shapes of particle tips were used.
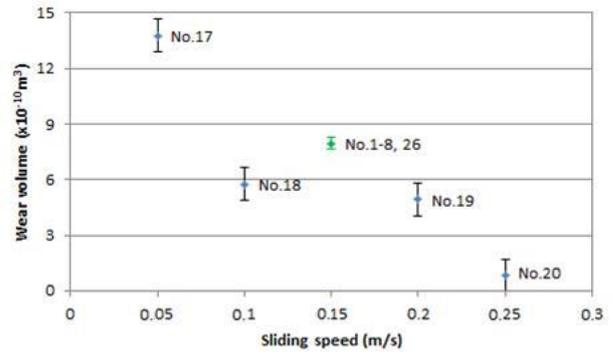
Fig. 18. Wear volume of particles as a function of sliding speed.
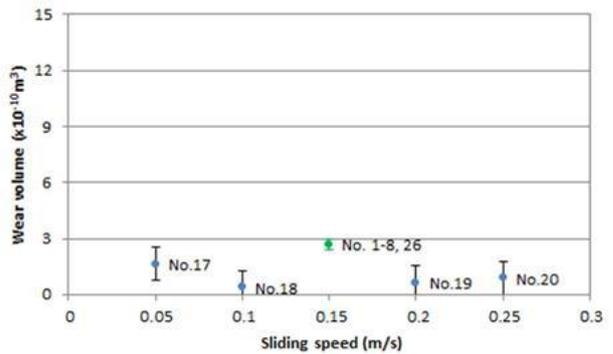
Fig. 19. Wear volume of mild steel disks as a function of sliding speed.

To verify the influence of inner structure and hardness of No. 17 particle on wear, the micro structure of particle No. 17 was examined after test, as shown in Fig. 15. The porous and uneven inner structure was observed under the microscope, which is believed to be the reason for the high wear volume of the particle [16,24]. The hardness of No. 17 particle is 450 ±75 (based on 16 test points and using 95 % confidence interval). This value is also no higher than the average in comparison with the frequency distribution of Sishen particles (Fig. 4). In line with previous research finding [18,25], when the ratio $H_p/H_d > 1.2$ the wear volumes for mild steel disks do not differ significantly. Based on this, it may be predicted that the sliding speed does not have significant influence for the tested low speeds.

However, it is noted that the wear for the practical speeds (e.g. conveyor speed 4-6 m/s) will be severer than that of experimental speeds (0.05-0.25m/s). This is ascribed to the fact that wear rate can be increased as contact temperature arises by friction heating under higher speeds [18]. The results of the tested sliding speeds cannot be directly used for

analyzing the practical situation. Nevertheless, it can provide reference for estimating the wear of industrial levels that have higher speeds.

3.4 Wear Subjected to Normal Forces: Series IV

Figures 20 and 21 respectively show the wear volumes of the particle and the mild steel of tests No. 21-24. The yellow areas are the wear volumes calculated by applying the coefficients of sliding wear $\alpha_{s,p} = (8.83 \pm 0.67) \times 10^{-13} \, m^2/N$ and $\alpha_{s,d} = (2.99 \pm 0.36) \times 10^{-13} \, m^2/N$ and for the distance 180 m. It shows that, by accounting for the variation of wear volume, all measured data can fall in the area of the predicted values by using Archard's equation (1). Therefore, it can be concluded that, although the wear of particles and mild steel undergo two wear states (Figs. 16 and 17), the cumulative wear volumes for long distances (such as 180 m) can be predicted by using the average coefficients of sliding wear and Archard's equation (1).
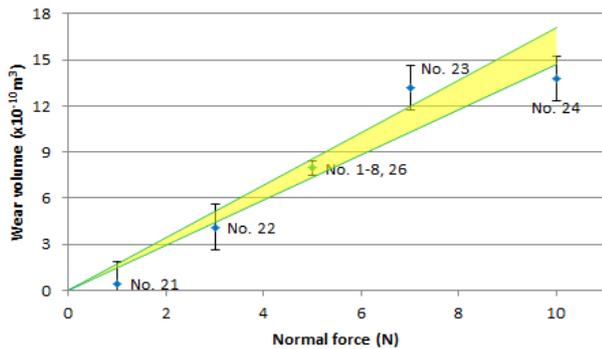
Fig. 20. Experimental and predicted wear volumes of particles as a function of normal force.
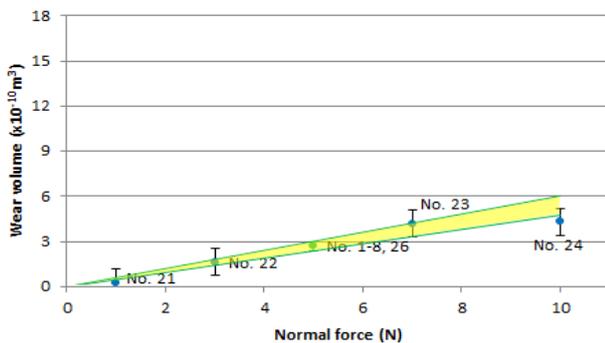
Fig. 21. Experimental and predicted wear volumes of mild steel disks as a function of normal force.

3.5 Characterization of Sliding Friction

The coefficient of sliding friction is defined as the ratio of tangential force to the normal force, and is given in equation (9),

$$\mu_s = \frac{F_t}{F_n} \qquad (9)$$

in which F_t is tangential force and F_n is indentation force. Due to the fact that shapes and hardness of particles are not constant, the coefficient of sliding friction varies with respect to sliding distance [26,27]. When the coefficient of sliding friction is plotted as a function of sliding distance, two types of friction characteristics (Type 1 and Type 2) are distinguished, as shown in Figs. 22 and 23.
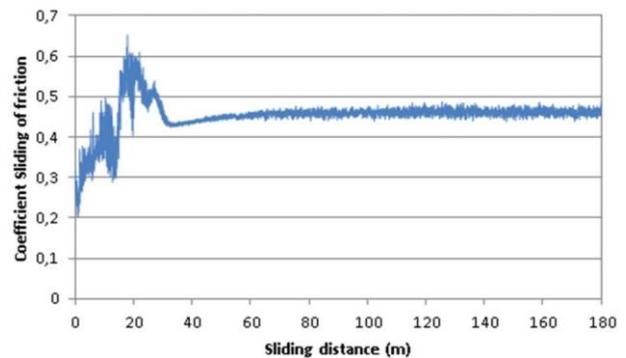
Fig. 22. Type 1 friction characteristics (test No. 3).
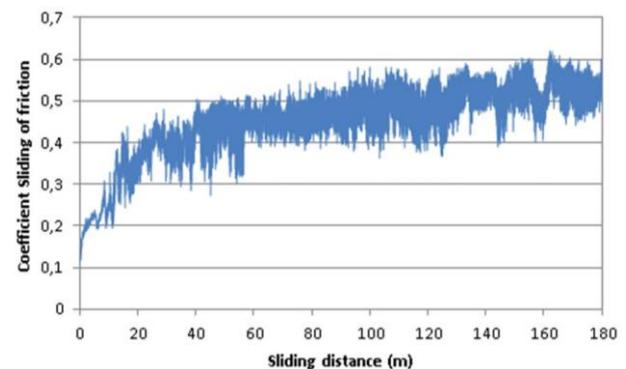
Fig. 23. Type 2 friction characteristics (test No. 7).

For Type 1, coefficient of sliding friction initially increases with certain fluctuations. After reaching a peak, it decreases and later maintains relatively a stable value. Type 1 friction curve is plotted by using the result of test No. 3, however, this type applies to majority tests when relatively low normal forces are applied [15]. By comparison, Type 2 (Fig. 23) has no peak value at the initial wear stage. With increasing sliding distance, the friction undergoes slight increase and tends to be stabilized. The slightly increasing trend might be due to the contact between particles and wear debris. The occurrence for Type 2 friction is believed that the particle has low hardness and thus is easily worn. By examining the hardness and the inner

surface structure of No. 3 and No. 7 particles, it is obtained that No. 7 particle has a lower hardness and a more porous inner structure than No. 3 particle.

Because the particles have different shapes, hardness and inner structure, the coefficient of sliding friction can vary significantly when subjecting to different distances and different particles. By comparing the friction characteristic with wear volumes as functions of sliding distance (Figs. 16 and 17), it can be concluded that when the coefficient of sliding friction reaches relatively steady state, wear also approaches a steady-state. Based on this, it is obtained that the maximum coefficients of sliding friction subjected to transient-state are 0.6-0.8. For the wear at steady-state of both Types 1-2, the maximum coefficients of sliding friction are 0.4-0.6. In addition, it is obtained that for majority tests the maximum sliding distances for transient state are between 20 and 80 m.

3.6 Characterization of Temperature Rise

Figure 24 shows an image of the thermal field during a pin-on-disk wear test. The points 1 and 2 are chosen at the proximity area of contact. Other points 3 and 4 and a square area 1 (which can monitor average temperature) are used for obtaining referential (room) temperature. By the thermal field, it can be concluded that a higher temperature occurs to pin particle than that of mild steel disk surface.

Fig. 24. Temperature measurement based on thermal field.

Figure 25 illustrates the temperature rise as a function of sliding distance for the particle of No. 26. It shows that the contact temperature initially increases then reaches a relatively steady value. By comparing the characteristics of temperature rise with corresponding wear

volumes (Figs. 16 and 17), it demonstrates that the characteristic of temperature rise is consistent with the wear rate at transient state and steady state based on the corresponding characteristics of sliding friction, as was also obtained by the sliding wear research of brass-steel pair and bronze-steel pair [9]. To verify the experimentally measured temperature rise, the theoretical calculations are done as below.
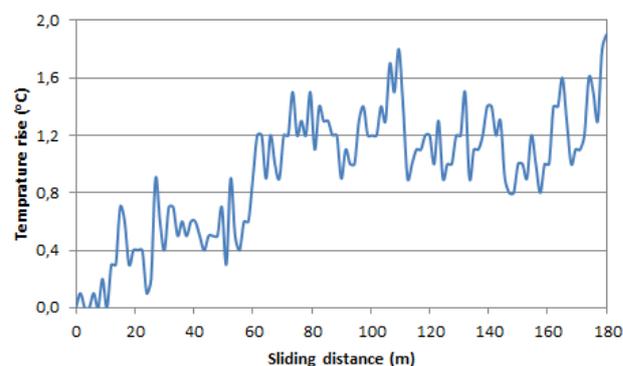
Fig. 25. Evolution of contact temperature rise for test No. 26.

The increase of contact temperature Tc can be estimated using equation (10) [28],

$$\frac{1}{\Delta T} = \frac{1}{\Delta T_p} + \frac{1}{\Delta T_d} \tag{10}$$

where T_p and T_d are temperature rise for particle and mid steel disk, which is respectively calculated based on the assumption that all generated heat is either dissipated at particle tip or to mild steel disk.

For the stationary particle, the average temperature rise ΔT_p is estimated by [28],

$$\Delta T_p = 0.5NL \tag{11}$$

where N is estimated temperature irrelative of sliding speed, and L is a dimensionless parameter. N and L are respectively given by equations (12) and (13) [28,29],

$$N = \frac{\pi \mu_s F_n}{\rho c A_0} \tag{12}$$

$$L = \frac{v_s a \rho c}{2k} \tag{13}$$

in which c is specific heat; A_0 is nominal contact area and k is thermal conductivity. For the test No. 26, A_0 is estimated as a circle area with radius a [26], i.e.

$$A_0 = \pi a^2 \qquad (14)$$

For the estimation of temperature rise of the moving mild steel disk (ΔT_d) which has moderately high speed, equation (15) is used [28].

$$\Delta T_d = \begin{cases} 0.5NL, & 0 < L < 0.1 \\ 0.5NLf(L), & 0.1 \le L \le 5 \end{cases} \qquad (15)$$

where $f(L)$ is a function of L. The selected values of $f(L)$ for equation (15) are presented in Table 2 [30].

Table 2. Function of $f(L)$ with respect to L [30].

L	0.1	0.2	0.5	1	2	5
f(L)	0.85	0.83	0.75	0.66	0.57	0.44

The values for estimating temperature rise of test No. 26 are summarized in Table 3 and 4.

Table 3. Values for material parameters.

Wear bodies	Material parameters		
	Density ρ	Specific heat h_c	Thermal conductivity k
Particle	4865	472 [31]	18 [31]
Disk	7932	490 [31]	54 [31]

Table 4. Values for contact parameters.

Wear bodies	Contact prameters			
	Friction μ_s	Force F_n	Velocity v_s	Area a
Particle	0.5	5	0.15	0.0004
Disk				

Using equations 11-14 and Table 3, it is calculated ΔT_p = 13.0 °C. Using equations 12-15 and Tables 2-3, it is obtained that ΔT_d = 2.5 °C. With the obtained T_p and T_d, and using equation (10), the contact temperature rise ΔT = 2.1 °C. This value is slightly higher than the maximum temperature rise estimated in Fig. 25. The reason is suggested to be the heat loss toward surroundings (i.e., ambient air and wear debris). Thus it illustrates that the temperatures of the pin-on-disk wear system has been successfully measured. For all the tests, the obtained range of temperature rise is 1.3-2.2 °C. Under this range of temperature rise, the sliding wear rate hardly changes [18,32]. Due to the fact that contact temperature will increase at higher speeds [32], it is inferred that, under bulk solids handling conditions the higher speeds result in severe wear volume than the experimental results.

4. CONCLUSIONS

In order to estimate the sliding wear in iron ore handling, pin-on-disk tests were carried out to determine the coefficient of sliding wear using Sishen particles and mild steel surfaces. Three conclusions are drawn below.

1. The average coefficients of sliding wear α for Sishen particle and mild steel are (8.83 ±0.67)×10⁻¹³ m²/N and (2.99 ±0.36)×10⁻¹³ m²/N based on 95 % confidence interval.

2. The sliding wear rates of Sishen particle and mild steel disk are different from transient-state to steady-state. The average coefficients of sliding wear for both Sishen particle and mild steel are capable of predicting wear volume subjected to long sliding distance of steady-sate.

3. Two types of sliding friction curves are distinguished. The maximum coefficient of friction for Type 1 occurs at the transient-state, and for Type 2 occurs at the steady-state. The contact temperature increases during the transient-state and stabilizes during the steady-state. The temperature rise has negligible influence on particle sliding wear for the tested low speeds.

REFERENCES

[1] D.J.C. Taylort, D.C. Page and P. Geldenhuys, 'Iron and steel in South Africa', *Journal of South African Institute of Mining and Metallurgy*, vol. 88, no. 3, pp. 73–95, 1988.

[2] A.W. Roberts and S.J. Wiche, 'Prediction of lining wear life of bins and chutes in bulk solids handling operations', *Tribolology International*, vol. 26, no. 5, pp. 345–351, 1993.

[3] J.F. Archard, 'Contact and rubbing of flat surfaces', *Journal of Applied Physics*, vol. 24, no. 8, pp. 981–988, 1953.

[4] J.M. Challen, P.L.B. Oxley and B.S. Hockenhull, 'Prediction of Archard's wear coefficient for metallic sliding friction assuming a low cycle fatigue wear mechanism', *Wear*, vol. 111, no. 3,

pp. 275–288, 1986.

[5] P. Lacey and S.A. Torrance, 'The calculation of wear coefficients for plastic contacts', *Wear*, vol. 145, pp. 367–383, 1991.

[6] L.J. Yang, 'An Integrated Transient and Steady-State Adhesive Wear Model', *Tribology Transactions*, vol. 46, no. 3, pp. 369–375, 2003.

[7] L.J. Yang, 'Determination of Steady-State Adhesive Wear Rate', *Journal of Tribology*, vol. 128, no. 4, p. 725, 2006.

[8] C.S. Ramesh, A.R.A. Khan, N. Ravikumar and P. Savanprabhu, 'Prediction of wear coefficient of Al6061-TiO2 composites', *Wear*, vol. 259, no. 1–6, pp. 602–608, 2005.

[9] M. Amiri, M.M. Khonsari and S. Brahmeshwarkar, 'On the relationship between wear and thermal response in sliding systems', *Tribology Letters*, vol. 38, no. 2, pp. 147–154, 2010.

[10] S.Y. Yau, T.H. Kim, S.S. Yoo and D.E. Kim, 'Fundamental investigation of micro-scale wear characteristics of ultra-fine gold wires under low contact force and long sliding distance', *Wear*, vol. 348–349, pp. 1–9, 2016.

[11] H. Siemes, 'Microstructure and crystallographic preferred orientation (CPO) of hematite ores from the Sishen Mine, Northern Cape', *South African Journal of Geology*, vol. 116, no. 1, pp. 79–100, 2013.

[12] ASTM G-99-95a, Standard Test Method for Wear Testing with a Pin-on-Disk Apparatus, pp. 1-5, 2000.

[13] M.O. Shabania and A. Mazahery, 'Development of an Extrusion Process to Ameliorate the Tribological Properties of Heat Treated Al Mg Si(Cu) System Alloys Matrix Composites in Consolidated State', *Tribology in Industry,* vol. 34, No. 3, pp. 166-173, 2012.

[14] M.R. Rahimipour, A.A. Tofigh, M.O. Shabani and P. Davami, 'The enhancement of wear properties of compo-cast A356 composites reinforced with Al2O3 nano particulates', *Tribology in Industry,* vol. 36, No. 2, pp. 220-227, 2014.

[15] A. Elhadi, A. Bouchoucha, W. Jomaa, Y. Zedan, T. Schmitt and P. Bocher, 'Study of surface wear and damage induced by dry sliding of tempered AISI 4140 steel against hardened AISI 1055 steel', *Tribology in Industry*, vol. 38, no. 4, pp. 475–485, 2016.

[16] G.B. Stachowiak and G.W. Stachowiak, 'The effects of particle characteristics on three-body abrasive wear', *Wear*, vol. 249, no. 3–4, pp. 201–207, 2001.

[17] J.J. Coronado, S.A. Rodríguez and A. Sinatora, 'Effect of particle hardness on mild-severe wear transition of hard second phase materials', *Wear*, vol. 301, no. 1-2, pp. 82-88, 2013.

[18] P.C. Okonkwo, G. Kelly, B.F. Rolfe and M.P. Pereira, 'The effect of sliding speed on the wear of steel-tool steel pairs', *Tribology International*, vol. 97, pp. 218–227, 2016.

[19] X.D. Niu, D.Q. An, X. Han, W. Sun, T.F. Su, J. An, and R.G. Li, 'Effects of Loading and Sliding Speed on the Dry Sliding Wear Behavior of Mg-3Al-0.4Si Magnesium Alloy', *Tribology Transactions*, vol. 60, no. 2, pp. 238–248, 2017.

[20] M. Banjac, A. Vencl and S. Otovic, 'Friction and Wear Processes – Thermodynamic Tribology in Industry', *Tribology in Industry.* vol. 36, no. 4, pp. 341–347, 2014.

[21] F.E. Kennedy, 'Thermal and thermomechanical effects in dry sliding', *Wear*, vol. 100, pp. 453–476, 1984.

[22] S.W. Lommen, 'Virtual prototyping of grabs: Co-simulation of discrete element method and rigid body models', *PhD thesis*, Faculty of Mechanical, Maritime and Materials Engineering, Delft University of Technology, Delft, 2016.

[23] N. Kumar, R.K. Gautam and S. Mohan, 'Wear and Friction Behavior of in-situ AA5052 / ZrB 2 Composites under Dry Sliding Conditions', *Tribology in Industry*, vol. 37, no. 2, pp. 244–256, 2015.

[24] A.J. Raj, A. Pottirayil and S. V. Kailas, Dry Sliding Wear Behavior of Ti-6Al-4V Pin Against SS316L Disk at Constant Contact Pressure, *Journal of Tribology*, vol. 139, no. 2, p. 21603, 2016.

[25] G. Straffelini, D. Trabucco and A. Molinari, 'Oxidative wear of heat-treated steels', *Wear*, vol. 250, no. 1–12, pp. 485–491, 2001.

[26] A. Jourani and S. Bouvier, 'Friction and Wear Mechanisms of 316L Stainless Steel in Dry Sliding Contact: Effect of Abrasive Particle Size', *Tribology Transactions*, vol. 58, no. 1, pp. 131–139, 2015.

[27] G. Pintaude, D.K. Tanaka and A. Sinatora, 'The effects of abrasive particle size on the sliding friction coefficient of steel using a spiral pin-on-disk apparatus', *Wear*, vol. 255, no. 1–6, pp. 55–59, 2003.

[28] J.F. Archard, 'The temperature of rubbing surfaces', *Wear*, vol. 2, no. 6, pp. 438–455, 1959.

[29] M.F. Ashby, J. Abulawi and H.S. Kong, 'Temperature Maps for Frictional Heating in Dry Sliding', *Tribol. Trans.*, vol. 34, no. June 2015, pp. 577–587, 1991.

[30] I. On, 'Estimation of flash temperatures in dry sliding', *Proc IMechE Part C: J Mechanical Engineering Science*, vol. 198, no. 8, pp. 91–97, 1984.

[31] Engineering Tool Box. [Online]. Available:http://www.engineeringtoolbox.com/. [Accessed: 20-Jul-2001].

[32] P.C. Okonkwo, G. Kelly, B.F. Rolfe and M.P.

Pereira, 'The effect of temperature on sliding wear of steel-tool steel pairs', *Wear*, vol. 282–283, pp. 22–30, 2012.

Nomenclature

a radius of a circular area of contact [m]

A_0 contact area between particle tip and a flat surface [m²]

B volume at the junctions at zero sliding distance [m³]

c specific heat [W/(kg·K)]

C experimental constant in the equation for estimating transient wear [1/m]

d diameter of particle [m]

$f(L)$ a function with respect to L [-]

H hardness [Pa]

H_e, H_p hardness of mild steel equipment and particle [Pa]

k thermal conductivity [W/(m·K)]

K dimensionless coefficient in Archard's equation [-]

L dimensionless parameter [-]

m_0, m_1 mass before test and after test [kg]

N parameter in evaluating temperature rise [oC]

F_n, F_t normal and tangential forces [N]

l sliding distance [m]

l_t, l_s sliding distance corresponding to transient-wear and steady-wear [m]

ΔT temperature rise [oC]

v relative velocity [m/s]

W_V wear volume [m³]

$W_{V,t}$ wear volume for transient-state [m³]

W_d, W_p wear volume of mild steel disk and particle [m³]

α_s coefficient of sliding wear [m²/N]

$\alpha_{s,p}, \alpha_{s,d}$ coefficient of sliding wear for Sishen particle and mild steel disk [m²/N]

μ_s coefficient of sliding friction [-]